RSC Advances

PAPER

View Article Online
View Journal | View Issue

CrossMark click for updates

Cite this: *RSC Adv.*, 2014, **4**, 51381

Poly(vinyl alcohol) electrospun nanofibrous membrane modified with spirolactam–rhodamine derivatives for visible detection and removal of metal ions†

Zhen Wei,[abc] Hui Zhao,[ac] Jianhua Zhang,[a] Liandong Deng,[a] Siyu Wu,[b] Junyu He[b] and Anjie Dong*[ac]

Poly(vinyl alcohol) electrospun nanofibrous (PVANF) membranes that could sensitively detect and adsorb metal ions were modified with spirolactam–rhodamineine derivatives (PVANF–SRD) membranes and sulfo-spirolactam–rhodamine derivatives (PVANF–SSRD) membranes. Surface chemistry and morphology during functionalization of PVANF membranes were monitored using Fourier transform-infrared spectroscopy (FT-IR), X-ray photoelectron spectroscopy (XPS) and scanning electron microscopy (SEM). These two membranes could display real-time sensing by the naked eye based on ring-opening reaction of spirolactam–rhodamine derivatives induced by corresponding metals. PVANF–SRD and PVANF–SSRD membranes exhibited high selectivity and sensitivity toward Fe^{3+}/Cr^{3+} and Hg^{2+}, respectively. In terms of PVANF–SSRD membranes, adsorption capacity for Hg^{2+} in contaminated water was studied. Freundlich isotherm could better describe the interactions than Langmuir: $K_f = 7.0175$ mg g^{-1} ($r^2 = 0.9996$) for Hg^{2+}. The regenerability of these two membranes was investigated *via* Na_4EDTA solution treatment, and results demonstrated good sustainability in detection and adsorption efficiency.

Received 23rd July 2014
Accepted 26th September 2014

DOI: 10.1039/c4ra07505f

www.rsc.org/advances

Published on 26 September 2014. Downloaded by Michigan State University on 21/01/2016 21:13:13.

1. Introduction

Metal ions play important roles in the human body as well as ecological systems.[1] Some metal ions are essential for maintaining health, such as ferric and chromium(III) ions, whereas other metal ions such as mercury(II) ions could cause serious diseases in the central nervous and endocrine systems.[2–4] Therefore, practical solutions that could easily detect and selectively quickly dispose of metal ions are urgently needed. For detection purposes, rhodamine B is well-known and extensively used as a fluorochrome due to its remarkable properties such as a high adsorption coefficient, high fluorescent quantum yield, and excitation and emission within visible wavelengths.[5] In particular, non-fluorescent spirolactam–rhodamineine derivatives obtained *via* the reaction of rhodamine B with primary amine derivatives can respond to certain metal ions to give strong fluorescence emissions.[6] Recently, several spirolactam–rhodamineine derivatives based on off–on fluorescent sensors have been developed for sensing metal ions, including Cu^{2+}, Hg^{2+}, Fe^{3+} and Cr^{3+} and so on.[7–18] All such sensors work *via* transition from the spirolactam form to a ring-open form upon binding captions, resulting in fluorescence enhancement (550–600 nm).

Although some materials functionalized by spirolactam–rhodamineine derivatives were prepared to detect metal ions or for adsorption purposes,[19–25] electrospun membrane adsorption or filtration became one of the most attractive methods in wastewater decontamination because of large specific-surface areas.[26–28] Electrospinning is a highly versatile method to process fibers with diameters ranging from nanometers to micrometers.[29–31] With different functional groups, electrospun fibers can be fabricated into sensor or adsorption materials with high sensitivity, fast response time and adsorbing capacity for metal ions or molecules in raw sewage.[32,33] Due to good film-forming ability and abundant hydroxyl groups for easy modification, water-stable poly(vinyl alcohol) (PVA) is one of the promising candidates for fabrication of sensing or adsorption membranes.[32–35] Even though the cross-linking is fully based on reactions with hydroxyl groups, there are still abundant active hydroxyls on the surface of nanofibers for subsequent reactions of functionalizing PVA membranes with specific detection groups. Grafting rhodamine derivatives on the surface of PVA

[a]*Department of Polymer Science and Technology and Key Laboratory of Systems Bioengineering, Ministry of Education, School of Chemical Engineering and Technology, Tianjin University, Tianjin 300072, China. E-mail: ajdong@tju.edu.cn; Fax: +86 022 27890706; Tel: +86 022 27890706*

[b]*Department of Applied Chemistry, College of Basic Science, Tianjin Agricultural University, Tianjin 300384, China*

[c]*Collaborative Innovation Center of Chemical Science and Engineering (Tianjin), Tianjin 300072, China*

† Electronic supplementary information (ESI) available: National Natural Science Foundation of China (51103097). See DOI: 10.1039/c4ra07505f

Published on 26 September 2014. Downloaded by Michigan State University on 21/01/2016 21:13:13.

nanofibrous membrane, compared with another matrix such as Fe_3O_4 nanoparticles in peer reports,[19–23] makes fluorescent-modified product possible for naked-eye detection. Moreover, PVA membrane-grafting rhodamine derivatives could be recycled with aqueous NaOH or Na_4EDTA treatment. Colour changes during adsorption or desorption process are observable.

For removal of metal ions, more effective, lower-cost methods to obtain clean water are of great importance. Traditionally, detection and separation/removal of metal ions were performed separately. Adsorption material detectable *via* the naked eye may save precious time in emergency situations. In our study, PVA electrospun nanofibrous membranes modified with two different rhodamine derivatives were designed and investigated for the first time. The objective of our work is to develop a facile strategy of practical regenerable materials for naked-eye metal ion sensing and removal with ultra-high sensitivity, selectivity and adsorption ability.

2. Materials and methods

2.1 Materials

Poly(vinyl alcohol) (1799 alcoholysis: 99.8–100% (mol mol^{-1})), glutaraldehyde (50% in H_2O), and epichlorohydrin were supplied by Shanghai Jingchun Industrial Co. Chloride salts for metal ions (K^+, Mg^{2+}, Ca^{2+}, Mn^{2+}, Co^{2+}, Ni^{2+}, Cu^{2+}, Zn^{2+}, Cd^{2+}, Hg^{2+}, Cr^{3+}, Fe^{3+}) and nitrate salts of a metal ion (Ag^+) were purchased from Sigma-Aldrich Co. All chemicals were analytical reagent grade and used as supplied. As shown in Scheme 1(A), spirolactam–rhodamine derivatives (SRD) and sulfo-spirolactam–rhodamine derivatives (SSRD) were synthesized according to the literature and confirmed by ^1H NMR and MS. The results were in agreement with a previous report.[37]

2.2 Preparation of water-stable poly(vinyl alcohol) electrospun nanofiber (PVANF) membrane

PVANF membrane was prepared according to a previous report with slight modifications.[36] PVA-1799 was dissolved in distilled water and refluxed for 1 h to obtain a homogenous solution with a concentration of 10 wt%. Subsequently, 25 wt% (based on the mass of PVANF) glutaraldehyde (GA) was added to the above solution under magnetic stirring for 0.5 h before electrospinning. The resulting solution was placed into a 10.0 mL syringe with a 7-gauge blunt-end needle, and the syringe was mounted in a syringe pump (74900-05, Cole-Parmer, USA) to deliver the solution at the speed of 0.5 mL h^{-1}. The high voltage and distance between needle tip to the collector were 13 kV and 20 cm, respectively. All fibers were fabricated at 25 °C and relative humidity of 40%. Freshly prepared PVANF/GA nanofibrous membranes were immersed in a mixed solution containing 10 vol% of HCl aqueous solution (37 wt%) and 90 vol% methanol for 9 days to obtain water-stable nanofibrous membrane.

2.3 Modification of poly(vinyl alcohol) electrospun nanofiber with rhodamine derivatives and sulfo-rhodamine derivatives

A preweighed PVANF membrane was immersed in 100 mL of NaOH solution (pH = 9–11). 7.0 mL of epichlorohydrin were added. The mixture was placed in an incubator shaker at 60 °C for 6 h and thoroughly washed with distilled water. The membrane was then immersed into water–ethanol (1 : 1 v/v) solution with 0.3% (w/v) spirolactam–rhodamine derivatives (SRD) and sulfo-spirolactam–rhodamine derivatives (SSRD), respectively. Subsequently, the pH value of above solution was adjusted to 9–11 *via* a 10 wt% NaOH solution. The mixture was placed in an incubator shaker at 60 °C for 12 h and then rinsed with distilled water and ethanol three times and dried with nitrogen. Finally, the PVANF–SRD and PVANF–SSRD membrane were obtained.

2.4 Characterization

The overall morphology of nanofibrous membranes was determined *via* scanning electron microscopy (SEM, S-4800, Hitachi, Japan). The average diameters of the obtained nanofibers were calculated directly with the SEM micrographs using Image Pro

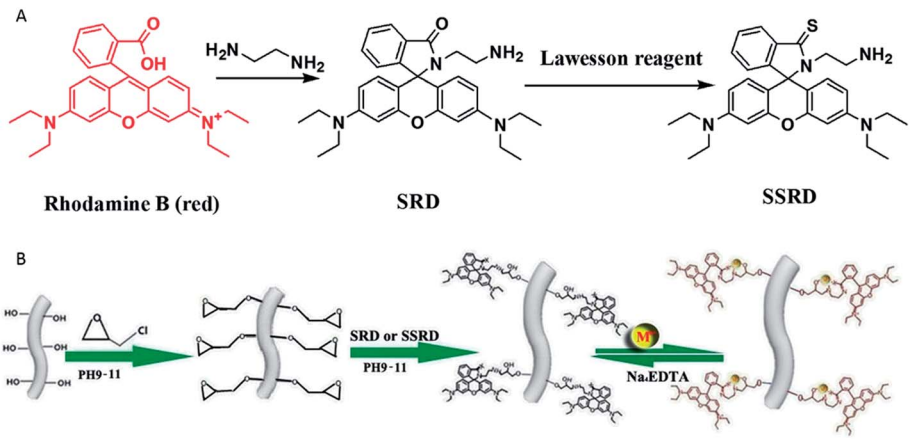

Scheme 1 Synthetic route of SRD and SSRD (A), schematic illustration of the functionalization of a poly(vinyl alcohol) electrospun nanofiber membrane by SRD (X = O, M^{n+} = Fe^{3+} or Cr^{3+}) or SSRD (X = S, M^{n+} = Hg^{2+}) and metal detection/adsorption applications (B).

 This journal is © The Royal Society of Chemistry 2014

Published on 26 September 2014. Downloaded by Michigan State University on 21/01/2016 21:13:13.

Plus 6 software. The BET surface area was obtained from N_2 adsorption–desorption isotherms measured using a surface area and porosity measurement system (TriStar II 3020 V1.03, Micromeritics, USA). The Fourier transform infrared (FTIR) spectra were characterized on an Affinity-1 FTIR spectroscopy from 4000 to 450 cm^{-1}. X-ray photoelectron spectra were obtained on an X-ray photoelectron spectrometer (XPS, ESCALabMKII, VG Scientific, UK), using the Al Kα X-ray source (1486.6 eV) as the exciting source. Ultraviolet-visible spectra (UV-vis) were recorded on a UV-1800 (Shimadzu, Japan) at room temperature. Fluorescence spectra were recorded on a RF-5301pc Fluorescence Spectrophotometer (Shimadzu, Japan).

2.5 Metal detection studies

To investigate the selectivity of PVANF–SRD and PVANF–SSRD membranes toward metal ions, various metal ion solutions were prepared in deionized water with the same concentration (1.0×10^{-3} M). The membranes were immersed in each solution for 10 min. After washing thoroughly with water, all membranes were dried with nitrogen. Fluorescence emission measurements were conducted. In order to investigate the sensitivity of PVANF–SRD membrane for Fe^{3+} and Cr^{3+} ions, PVANF–SRD membrane was immersed in different concentrations of Fe^{3+} and Cr^{3+} ions for 10 min. Afterwards, the membrane was washed thoroughly with deionized water, and the UV-vis absorption spectra and fluorescence spectra were measured. Similar procedures were performed with the PVANF–SSRD membrane at different Hg^{2+} ion concentrations.

2.6 Adsorption of Hg^{2+} from Haihe River samples

The adsorption capacities of the modified nanofibrous membranes were assessed by monitoring the residual amount of metal ions in sewage using inductively coupled plasma mass spectrometry (ICP-MS, Thermofisher, Germany). The water samples from Haihe River (Tianjin, China) were collected. Since no detectable mercury was in the samples, 0.2–2 mg of $Hg(NO_3)_2$ was added in 20 mL samples to simulate contaminated water. For Hg^{2+} detection and adsorption, 20 mg of PVANF–SSRD membrane (size around 12 × 12 cm) were immersed in the samples and agitated on a mechanical shaker between 5 and 120 min to adsorb Hg^{2+}. After removing the membrane, remnant Hg^{2+} was determined by ICP-MS. Equilibrium isotherms required for design and operation of the adsorbent to treat Hg^{2+} bearing wastewater were obtained.

The amount of Hg^{2+} adsorbed was calculated as follows:

$$q = \frac{C_0 - C_f}{M} \times V \quad (1)$$

where q is the amount of Hg^{2+} adsorbed (mg g^{-1}), C_f and C_0 are final and initial Hg^{2+} concentrations (mg L^{-1}), respectively; V is the volume of Hg^{2+} used (L); and M is the mass of adsorbent (g).

2.7 Reversibility of PVANF–SRD and PVANF–SSRD membrane samples

For the reversibility (reusability) of the PVANF–SRD and PVANF–SSRD membranes, the membranes were immersed in the saturated Na_4EDTA solution for 10 min, and then washed with methanol and water and dried with nitrogen.

3. Results and discussion

Scheme 1(A) showed the synthetic route of spirolactam–rhodamine derivatives (SRD) and sulfo-spirolactam–rhodamine derivatives (SSRD). As shown in Scheme 1(B), functionalization of the PVANF membrane by SRD or SSRD involves two steps. First, the epoxy group was grafted onto the PVANF membrane by reacting epichlorohydrin with –OH on the surface of the PVANF membrane in alkaline conditions, resulting in PVANF–O membrane. In the second step, the SRD and SSRD reacted with PVANF–O membrane to obtain the final PVANF–SRD and PVANF–SSRD membranes, respectively. The loadage of probe SRD and SSRD onto the PVANF membranes was equivalent to 9.2×10^{-5} M and 9.1×10^{-5} M, respectively, which were calculated based on absorbance of the PVANF–SRD or PVANF–SSRD membranes after immersion in saturated Fe^{3+} or Hg^{2+} solution.[25]

3.1 Morphological characterization

The morphologies of the products were observed by SEM. Fig. 1A shows a representative SEM image of the PVANF membrane. Fig. 1B–D depict representative SEM images of the intermediate (PVANF–O membrane) and final products (PVANF–SRD membrane, PVANF–SSRD membrane). The fiber sizes of the membranes were calculated as averages based on 100 measurements using Image Pro Plus 6 software. The average fiber diameters of PVANF–SRD membrane and PVANF–SSRD membrane were 290.11 nm and 287.88 nm, respectively, which were of no obvious difference from that of PVANF (271.40 nm) and PVANF–O (270.9 nm). The fiber integrity and porosity were maintained during functionalization. The surface area and pore size of PVANF–SRD membrane obtained were 18.78 m^2 g^{-1} and 143.85 Å, respectively. Similarly, the surface area and pore size of PVANF–SSRD membrane were 18.62 m^2 g^{-1} and 140.32 Å, respectively.

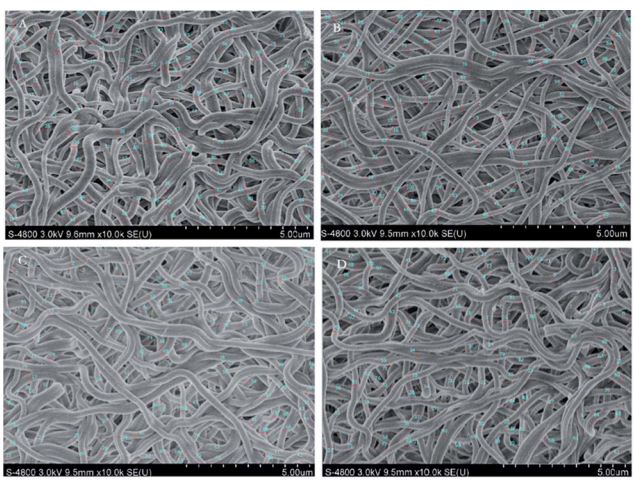

Fig. 1 SEM images of PVANF membrane (A), PVANF–O membrane (B), PVANF–SRD membrane (C), PVANF–SSRD membrane (D).

Published on 26 September 2014. Downloaded by Michigan State University on 21/01/2016 21:13:13.

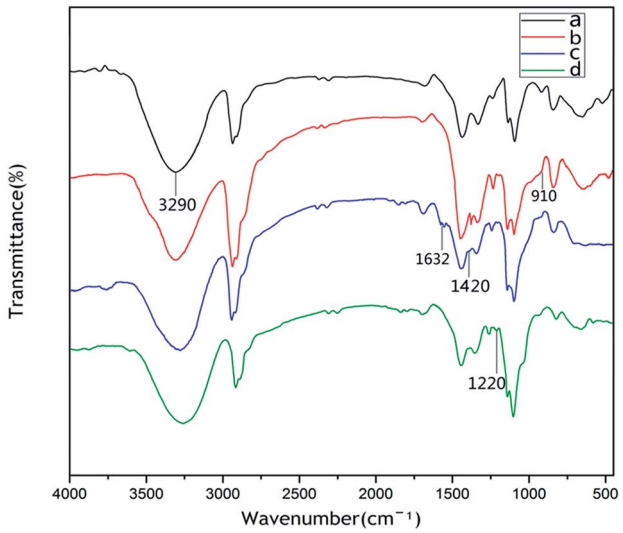

Fig. 2 FT-IR spectra of PVANF membrane (a), PVANF–O membrane (b), PVANF–SRD membrane (c), PVANF–SSRD membrane (d).

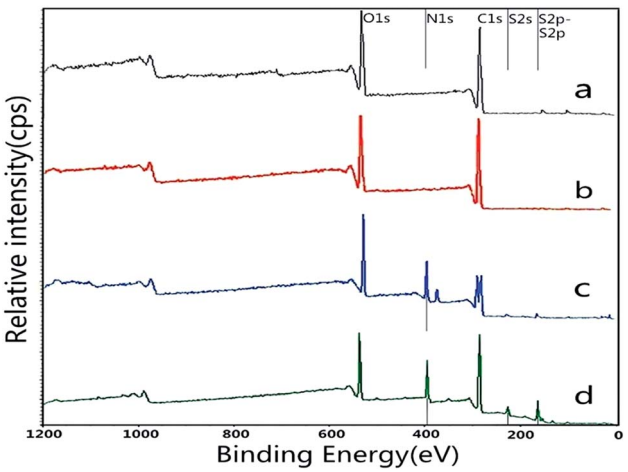

Fig. 3 C1s, N1s, O1s and S1s XPS for of PVANF membrane (a), PVANF–O membrane (b), PVANF–SRD membrane (c), PVANF–SSRD membrane (d).

3.2 Fourier transformation-infrared spectroscopy

Functionalization of the PVANF membrane by SRD and SSRD was confirmed by FTIR spectroscopy. Fig. 2 showed the FT-IR spectra of PVANF membrane (a), PVANF–O membrane (b), PVANF–SRD membrane (c), and PVANF–SSRD membrane (d) in the 450–4000 cm^{-1} wavenumber range. The peak at 3290 cm^{-1} in spectrum could be assigned to the –OH stretching vibration arising from surface hydroxyl groups of PVANF. The spectrum of the PVANF–O membrane showed the peak at 910 cm^{-1}, which was the characteristic peak of epoxide group, indicating formation of the epoxy group onto the PVANF membrane. The peaks at 1420 and 1632 cm^{-1} in the spectrum of Fig. 2c were assigned to the C–N and C=O stretching vibration, respectively, which indicated that the PVANF–SRD membrane was successfully fabricated. The increase in band intensity at 1220 cm^{-1} could be attributed to C=S stretching vibration of SSRD. Therefore, it can be concluded that SRD and SSRD had been grafted successfully onto the surface of PVANF membrane.

3.3 Surface composition investigation using X-ray photoelectron spectroscopy

XPS was used to identify the surface composition of both the PVANF–SRD and PVANF–SSRD membranes. Fig. 3 showed the C1s, N1s, O1s, S2s and S2p XPS for PVANF membrane (a), PVANF–O membrane (b), PVANF–SRD membrane (c), and PVANF–SSRD membrane (d). The surface of the PVANF–SRD membrane exhibited more apparent N1 content than the PVANF and PVANF–O membrane, which were attributed to SRD. Additional S1s and S2s that appeared in the XPS of PVANF–SSRD membrane were assigned to SSRD. The result also indicated that SRD and SSRD had been grafted successfully onto the surface of PVANF membrane.

3.4 Selectivity and sensitivity of PVANF–SRD and PVANF–SSRD membrane

Photos were taken when PVANF–SRD membranes were immersed in different metal ions (1.0×10^{-3} M) for 5 min (as shown in Fig. 4A). Significant colour transition from white to pink was instantly observed by the naked eye when the membrane was immersed in solution with Fe^{3+} or Cr^{3+}. As shown in Fig. 4B, photographs of the PVANF–SSRD membranes immersed in the aqueous solutions of various metal ions were examined for selectivity and visibility of metal ion detection. The PVANF–SSRD membrane showed comparatively high specificity toward Hg^{2+}.

Fluorescence intensity changes of PVANF–SRD membrane after immersion in each ion solution (1.0×10^{-3} M) for 10 min with excitation at 525 nm were measured (see Fig. 5A). The result clearly demonstrated that the PVANF–SRD membrane had excellent selectivity toward both Fe^{3+} and Cr^{3+} ions.

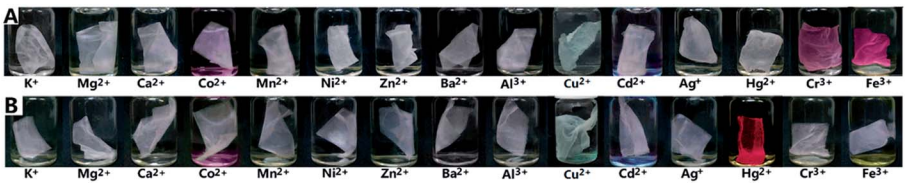

Fig. 4 Photographs of the PVANF–SRD membrane (A) and PVANF–SSRD membrane (B) immersed into K^+, Mg^{2+}, Ca^{2+}, Co^{2+}, Mn^{2+}, Ni^{2+}, Zn^{2+}, Ba^{2+}, Al^{3+}, Cu^{2+}, Cd^{2+}, Ag^+, Hg^{2+}, Cr^{3+}, Fe^{3+} aqueous solutions (1.0×10^{-3} M) for 5 min.

 This journal is © The Royal Society of Chemistry 2014

Published on 26 September 2014. Downloaded by Michigan State University on 21/01/2016 21:13:13.

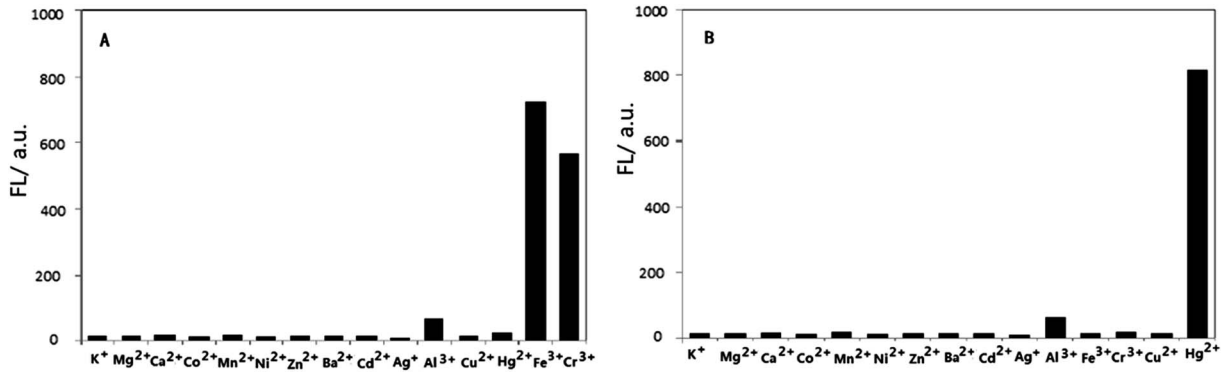

Fig. 5 Fluorescence intensity changes of the PVANF–SRD membrane (A) and PVANF–SSRD membrane (B) immersed into K^+, Mg^{2+}, Ca^{2+}, Co^{2+}, Mn^{2+}, Ni^{2+}, Zn^{2+}, Ba^{2+}, Cd^{2+}, Ag^+, Al^{3+}, Cu^{2+}, Hg^{2+}, Cr^{3+}, Fe^{3+} aqueous solutions (1×10^{-3} M, respectively) for 10 min ($\lambda_{exc} = 525$ nm).

PVANF–SSRD selectivity and sensitivity for mercury ion sensing were also examined following a similar procedure (see Fig. 5B).

As seen in Fig. 6, the coexistence of most selected metal ions did not interfere with either Fe^{3+} or Cr^{3+} detection of PVANF–SRD membrane. Meanwhile, coexistences had negligible interference effect on Hg^{2+} sensing by the PVANF–SSRD membrane.

The UV-vis spectrum of the membrane was measured after immersed in different concentrations of Fe^{3+} and Cr^{3+} aqueous solutions (Fig. 7A and B). The result indicated that with the increase of Fe^{3+} or Cr^{3+} concentration in aqueous solutions, the absorption spectrum at around 560 nm also increased, which coincided with the adsorption of rhodamine. Fig. 8A and B shows the fluorescence spectrum of the PVANF–SRD membrane after immersion in different concentrations of Fe^{3+} and Cr^{3+} aqueous solutions. It was found that the fluorescence intensity at 593 nm increased steadily as the concentration of Fe^{3+} or Cr^{3+} increased. Fe^{3+} induced stronger fluorescence intensity than that of Cr^{3+}. Results indicated that the PVANF–SRD membrane could be used as a dual response sensor with much faster response time for Fe^{3+} and Cr^{3+} detection and the detection limit was approximately 1.0×10^{-6} M for both Fe^{3+} and Cr^{3+}, which was comparable to other materials based on rhodamine derivatives in a previous report.[25] UV-vis absorption and fluorescence spectrum of PVANF–SSRD membrane after immersion

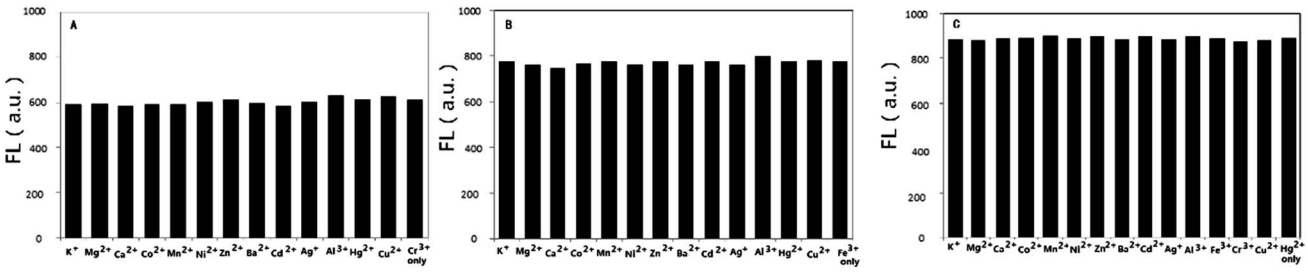

Fig. 6 Fluorescence intensity changes of the PVANF–SRD membrane after being immersed into the aqueous solution of chromium ions (A) or ferric ion (B) (1×10^{-3} M) only and aqueous coexistence solution containing K^+, Mg^{2+}, Ca^{2+}, Co^{2+}, Mn^{2+}, Ni^{2+}, Zn^{2+}, Ba^{2+}, Cd^{2+}, Ag^+, Al^{3+}, Hg^{2+}, Cu^{2+}(1×10^{-3} M), respectively; PVANF–SSRD membrane after being immersed into the aqueous solution of mercury ion (C) (1×10^{-3} M) and aqueous coexistence solution containing K^+, Mg^{2+}, Ca^{2+}, Co^{2+}, Mn^{2+}, Ni^{2+}, Zn^{2+}, Ba^{2+}, Cd^{2+}, Ag^+, Al^{3+}, Cu^{2+}, Fe^{3+},Cr^{3+} (1×10^{-3} M), respectively ($\lambda_{exc} = 525$ nm).

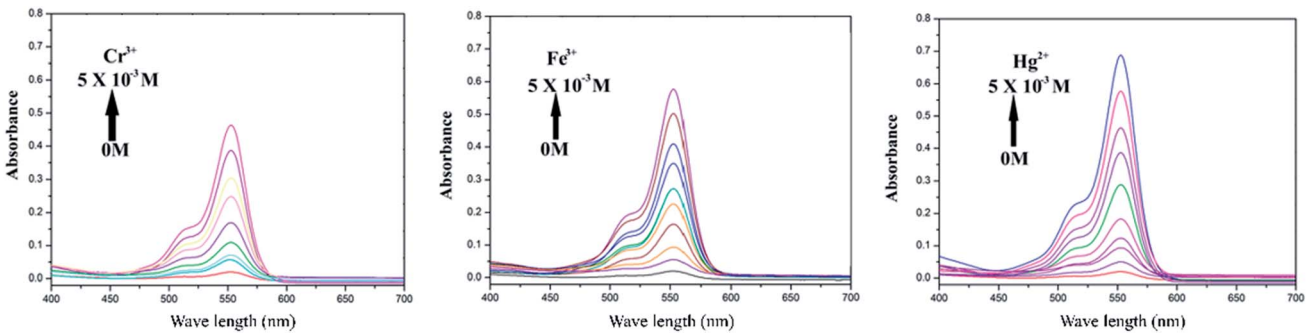

Fig. 7 UV-vis absorption spectra of the PVANF–SRD membrane after being immersed into Fe^{3+} (A) and Cr^{3+} (B) aqueous solutions; UV-vis absorption spectra of the PVANF–SSRD membrane after being immersed into Hg^{2+} (C) aqueous solutions for 10 min (pH = 7).

Published on 26 September 2014. Downloaded by Michigan State University on 21/01/2016 21:13:13.

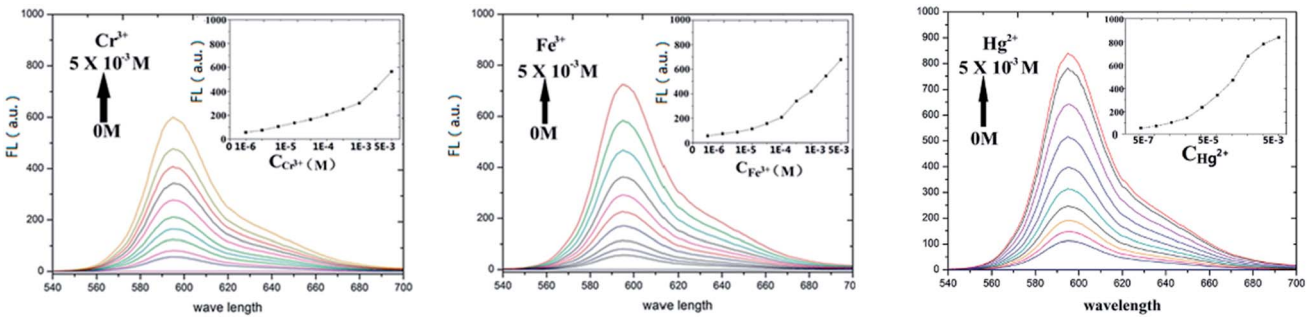

Fig. 8 Fluorescence spectra of the PVANF–SSRD membrane after being immersed into Fe^{3+} (A) and Cr^{3+}(B) aqueous solutions; PVANF–SSRD membrane after being immersed into Hg^{2+} (C) aqueous solutions ($\lambda_{exc} = 525$, pH = 7).

into different concentrations of Hg^{2+} aqueous solutions are shown in Fig. 7C and 8C. PVANF–SSRD displayed very good selectivity, sensitivity and fast response for Hg^{2+}. Compared with the PVANF–SRD membrane, the PVANF–SSRD membrane showed greater sensitivity to Hg^{2+} with the quantification limit at approximately 5.0×10^{-7} M.

3.5 Adsorption study

Contact time is a pertinent parameter that can determine adsorbent performance. Adsorption was monitored by immersing 20 mg of electrospun membranes into 20 mL of 0.2 mg $Hg(NO_3)_2$ solution. The amount of Hg^{2+} adsorbed by PVANF–SSRD and PVANF membranes was investigated as a function of contact time, as shown in Fig. 9. A high uptake rate observed for the first 10 min could be explained by the availability of many adsorption sites in the PVANF–SSRD membrane. As Hg^{2+} ions became attached to these sites with contact time, the amount of adsorbed Hg^{2+} gradually reached a maximum after which significant Hg^{2+} quantities were no longer removed; thus, equilibrium was established.

The equilibrium time for Hg^{2+} in PVANF–SSRD membrane was 20 min and in PVANF membrane 40 min (Fig. 9). The PVANF–SSRD membrane showed obvious improved adsorption compared to the PVANF membrane. This is explained by the high number of hydroxyl groups exposed for reaction with SSRD. After the equilibrium time occurred, the removal of Hg^{2+} was approximately 93%.

Langmuir and Freundlich models are commonly used for solid–liquid phase adsorption isotherms, which could describe the relationship between Hg^{2+} in solution and PVANF–SSRD membranes. The more appropriate model can reveal adsorption kinetics, as well as adsorption capacity, of functionalized nanofibrous membranes. It is assumed that every adsorption site is equivalent and the ability of a probe to bind is independent of whether or not adjacent sites are occupied.[26,38]

The Langmuir model is applicable in cases where a monolayer of adsorbed ions is formed at the membrane surface, while the Freundlich isotherm model is widely used for heterogeneous surfaces energies. The linearized form of the two adsorption isotherms models is defined by the following equations.

First is the Langmuir adsorption isotherm:

$$\frac{C_e}{q_e} = \frac{1}{q_{max}} C_e + \frac{1}{q_{max} K_L} \quad (2)$$

where C_e is the equilibrium concentration of adsorbate ions (mg L^{-1}), q_e is the amount of ions adsorbed at equilibrium (mg g^{-1}), q_{max} is the adsorption capacity of adsorbent (mg g^{-1}) and K_L is a Langmuir constant related to energy.

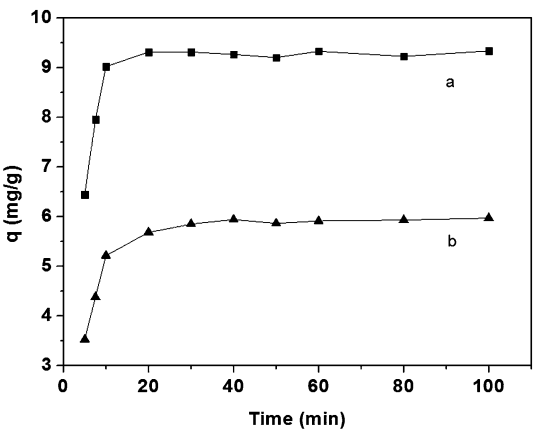

Fig. 9 Effect of contact time on adsorption of PVANF–SSRD membrane (a) and PVANF membrane (b).

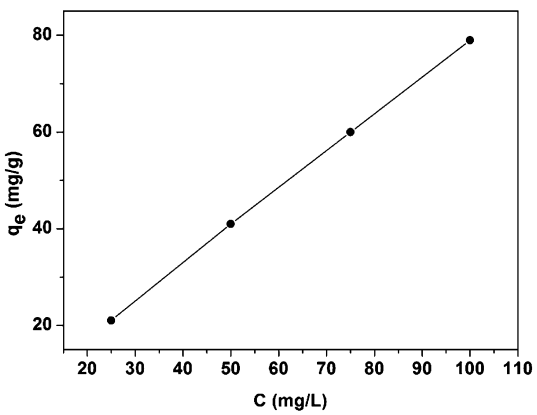

Fig. 10 Adsorption isotherm for Hg^{2+} with contact time 100 min, adsorbent concentration 1 g L^{-1}.

 This journal is © The Royal Society of Chemistry 2014

Published on 26 September 2014. Downloaded by Michigan State University on 21/01/2016 21:13:13.

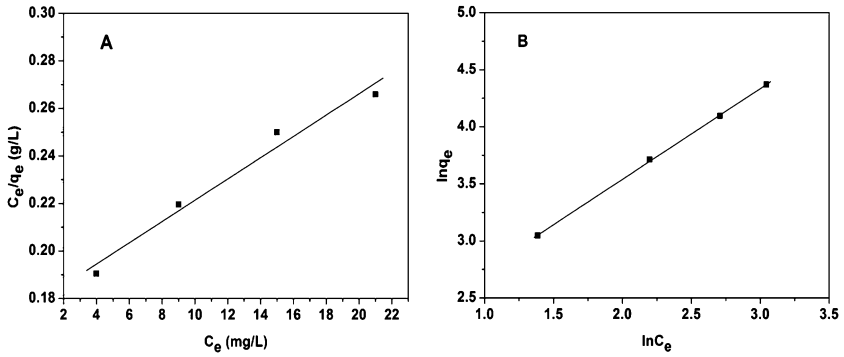

Fig. 11 (A) Langmuir and (B) Freundlich isotherms for Hg ions adsorption on PVANF–SSRD.

Table 1 Langmuir and Freundlich isotherm constants for Hg^{2+} of PVANF–SSRD and PVANF membranes

		Langmuir		Freundlich		
Metal ion	q_{max} (mg g^{-1})	K_L (L mg^{-1})	r^2	K_F (mg g^{-1})	n	r^2
Hg	222.23[a]	0.0255	0.9746	7.0175	1.26	0.9996
	69.93[b]	0.0073	0.9818	3.2446	1.60	0.9837

[a] PVANF–SSRD membrane. [b] PVANF membrane.

Table 2 Comparison of maximum adsorption capacity (mg g^{-1}) of PVANF–SSRD with other selected adsorbents

Adsorbent	Hg	Ref.
Sulfur-functionalized silica gels	47.8	39
Zonal thiol-functionalized silica nanofibers	57.5	40
PVA/PVI membrane	118.3	41
Organic–inorganic silica membrane (MCM-3T)	234.9	42
PVANF–SSRD membrane	222.2	This study

Next is the Freundlich adsorption isotherm:

$$\ln q_e = \ln K_f + \frac{1}{n} \ln C_e \quad (3)$$

where q_e and C_e assume the same quantities as in Langmuir, while K_f and n are adsorption capacity and adsorption intensity constants, respectively.[9]

The adsorption kinetics were studied using different concentrations for adsorbate metal ions—25, 50, 75 and 100 mg L^{-1}—at an adsorbent concentration of 1 g L^{-1}. The adsorption isotherms, Langmuir and Freundlich, are represented by Fig. 10 and 11, respectively.

The maximum adsorption (q_{max}) is reported in Table 1. The adsorption capacities of PVANF–SSRD are 222.23 mg g^{-1} for Hg^{2+}, compared to 69.93 mg g^{-1} for PVANF. Moreover, Table 1 showed that the metal uptake data agree strongly with the Freundlich adsorption isotherm model with correlation coefficient (r^2) of 0.9996. This supports the theory that the adsorption concluded the probe and physical adsorption. Moreover, the adsorption capacities of Hg^{2+} by PVANF–SSRD membranes were compared with selected adsorbents (Table 2). The table shows that PVANF–SSRD membranes have good potential for specific heavy metal adsorption in water.

3.6 Regeneration (reversibility) of PVANF–SRD membrane and PVANF–SSRD membrane

To investigate the reversibility and regeneration of PVANF–SRD membrane for Fe^{3+} and Cr^{3+} detection and adsorption, after immersing in Fe^{3+} or Cr^{3+} solutions until reaching equilibrium,

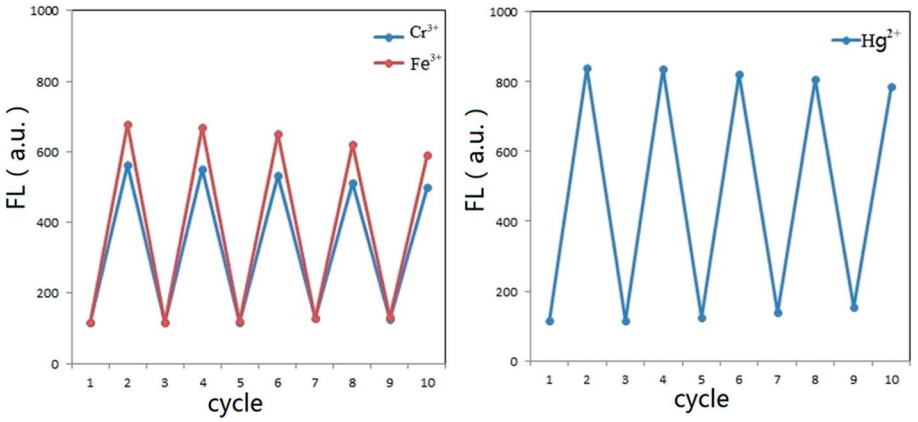

Fig. 12 Fluorescence intensity change for the PVANF–SRD membrane after alternate treatment by aqueous solution of Fe^{3+}/Cr^{3+} (1×10^{-3} M) and Na_4EDTA and PVANF–SSRD membrane after alternate treatment by aqueous solution of Hg^{2+} (1×10^{-3} M) and Na_4EDTA ($\lambda_{exc} = 525$ nm).

Published on 26 September 2014. Downloaded by Michigan State University on 21/01/2016 21:13:13.

PVANF–SRD membranes could be restored by exposed in NaOH or Na_4EDTA solution. The red colour faded completely within 10 min. These procedures were repeated 10 times and fluorescent emission signals measured at each stage (Fig. 12A). The open-ring-state rhodamine turned back to spirolactam due to its more stable form of SRD under alkaline conditions. Na_4EDTA could also restore the membrane using its more complex capacity with Fe^{3+} and Cr^{3+}. PVANF–SSRD membranes could also be reversed by exposure in Na_4EDTA solution, and its fluorescent intensity changed with alternately treated with Hg^{2+} ions and Na_4EDTA solutions (Fig. 12B). The results clearly demonstrated that these membranes could be reused several times without significant decline in detection and adsorption capacities.

4. Conclusions

In summary, two different spirolactam–rhodamineine derivatives were successfully functionalized on the surface of PVA electronspun nanofibrous membranes for Fe^{3+}/Cr^{3+} and Hg^{2+} sensing and adsorption purposes. These membranes displayed real-time sensing with good sensitivity and selectivity. Due to their large adsorption capacity, these factionalized membranes showed great potential for adsorption of specific heavy metals in water purification. It is also worth noting that the material could be recycled without significant reduction of its adsorption capacity. Colour changes can occur in the process of adsorption or desorption, which is convenient for applications in sewage treatment and reutilization. Modifying other metal ion fluorescent probes on the surface of nanofibers with such a facile strategy could facilitate expanding the range for both detection and adsorption purposes.

Notes and references

1 S. Toyokuni, *Cancer Sci.*, 2009, **100**, 9.
2 M. B. Zimmermann and R. F. Hurrell, *Lancet*, 2007, **370**, 511.
3 K. N. Jeejeebhoy, R. C. Chu and E. B. Marliss, *Am. J. Clin. Nutr.*, 1977, **30**, 531.
4 E. G. Pacyna and J. M. Pacyna, *Water, Air, Soil Pollut.*, 2002, **137**, 149.
5 Y. K. Yang, K. J. Yook and J. Tae, *J. Am. Chem. Soc.*, 2005, **127**, 16760.
6 H. N. Kim, M. H. Lee and H. J. Kim, *Chem. Soc. Rev.*, 2008, **37**, 1465.
7 Y. Xiang, A. Tong and P. Jin, *Org. Lett.*, 2006, **8**, 2863.
8 Y. Xiang, M. Li and X. Chen, *Talanta*, 2008, **74**, 1148.
9 H. Zheng, Z. H. Qian and L. Xu, *Org. Lett.*, 2006, **8**, 859.
10 B. P. Joshi, J. Park and W. I. Lee, *Talanta*, 2009, **78**, 903.
11 J. L. Chen, A. F. Zheng and A. H. Chen, *Anal. Chim. Acta*, 2007, **599**, 134.
12 J. Huang, Y. Xu and X. Qian, *J. Org. Chem.*, 2009, **74**, 2167.
13 C. C. Huang and H. T. Chang, *Anal. Chem.*, 2006, **78**, 8332.
14 Y. Xiang and A. J. Tong, *Org. Lett.*, 2006, **8**, 1549.
15 S. Bae and J. Tae, *Tetrahedron Lett.*, 2007, **48**, 5389.
16 J. Mao, L. Wang and W. Dou, *Org. Lett.*, 2007, **9**, 4567.
17 A. J. Weerasinghe, C. Schmiesing and E. Sinn, *Tetrahedron Lett.*, 2009, **50**, 6407.
18 P. Mahato, S. Saha and E. Suresh, *Inorg. Chem.*, 2012, **51**, 1769.
19 Y. Xu, Y. Zhou and W. Ma, *J. Nanopart. Res.*, 2013, **15**, 1716.
20 X. Peng, Y. Wang and X. Tang, *Dyes Pigm.*, 2011, **91**, 26.
21 Y. Xu, Y. Zhou and W. Ma, *Appl. Surf. Sci.*, 2013, **276**, 705.
22 M. Yin, Z. Li and Z. Liu, *ACS Appl. Mater. Interfaces*, 2012, **4**, 431.
23 Y. Chen and S. Mu, *Sens. Actuators, B*, 2014, **192**, 275.
24 W. Huang, D. Wu and G. Wua, *Dalton Trans.*, 2012, **41**, 2620.
25 B. Ma, S. Wu and F. Zeng, *Sens. Actuators, B*, 2010, **145**, 451.
26 M. Stephen, N. Catherine and M. Brenda, *J. Hazard. Mater.*, 2011, **192**, 922.
27 P. Chen, H. W. Liang and X. H. Lv, *ACS Nano*, 2011, **5**, 5928.
28 L. L. Wu, X. Y. Yuan and J. Sheng, *J. Membr. Sci.*, 2005, **250**, 167.
29 Z. M. Huang, Y. Z. Zhang and M. Kotaki, *Compos. Sci. Technol.*, 2003, **63**, 2223.
30 D. Li and Y. N. Xia, *Adv. Mater.*, 2004, **16**, 1151.
31 A. Greiner and J. H. Wendorff, *Angew. Chem., Int. Ed.*, 2007, **46**, 5670.
32 L. Jiang, H. Dong and W. Hu, *Soft Matter*, 2011, **7**, 1615.
33 C. H. Lee, S. K. Kang and J. A. Lim, *Soft Matter*, 2012, **8**, 10238.
34 C. Tang, C. D. Saquing and J. R. Harding, *Macromolecules*, 2010, **43**, 630.
35 B. Ding, H. Y. Kim and S. C. Lee, *J. Polym. Sci., Part B: Polym. Phys.*, 2002, **40**, 1261.
36 J. Wang, H. B. Yao and D. He, *ACS Appl. Mater. Interfaces*, 2012, **4**, 1963.
37 B. Liu, F. Zeng and G. Wu, *Chem. Commun.*, 2011, **47**, 8913.
38 Y. Bulut and Z. Baysal, *J. Environ. Manage.*, 2006, **78**, 107.
39 K. Johari, N. Saman and H. Mat, *J. Mater. Eng. Perform.*, 2014, **23**, 809.
40 S. Li, X. Yue and Y. Jing, *Colloids Surf., A*, 2011, **380**, 229.
41 H. Bessbousse, T. Rhlalou and J. F. Verchere, *Chem. Eng. J.*, 2010, **164**, 37.
42 Q. Zou, L. Zou and H. Tian, *J. Mater. Chem.*, 2011, **21**, 14441.

 This journal is © The Royal Society of Chemistry 2014